



Dynamic Simulation of Erosion and Redeposition on Plasma Facing Materials

Kaoru Ohya, *The University of Tokushima, Japan*
with Contributions by

T. Tanabe, *Kyushu University, Japan*

V. Philipps, A. Pospieszczyk, A. Kirshner, T. Hirai, and TEXTOR team,
Forshungszentrum Juelich, Germany

M. Rubel, *Royal Institute of Technology*

M. Wada, *Doshisha University, Japan*

T. Ohgo, *Fukuoka University of Education, Japan*

N. Noda, *National Institute for Fusion Science, Japan*

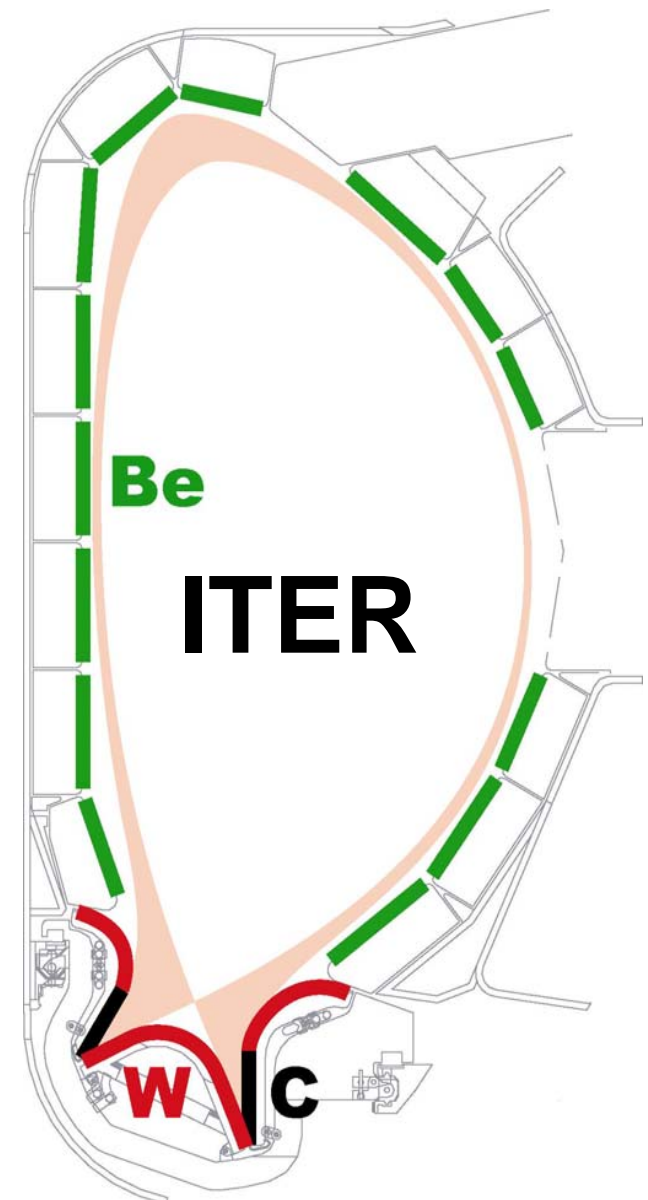
H. Takenaga, *Japan Atomic Energy Agency, japan*

K.Inai, S.Ebisu, H.Yoshioka, Y.Kikuhara, *The University of Tokushima, Japan*

Presented at 1st NIFS-CRC International Symposium and 1st Korea-Japan Workshop on "Edge-Plasma and Surface Component Interactions in Steady State Magnetic Fusion Devices", NIFS, May 20 - 22, 2007

Some plasma wall interaction issues for ITER :

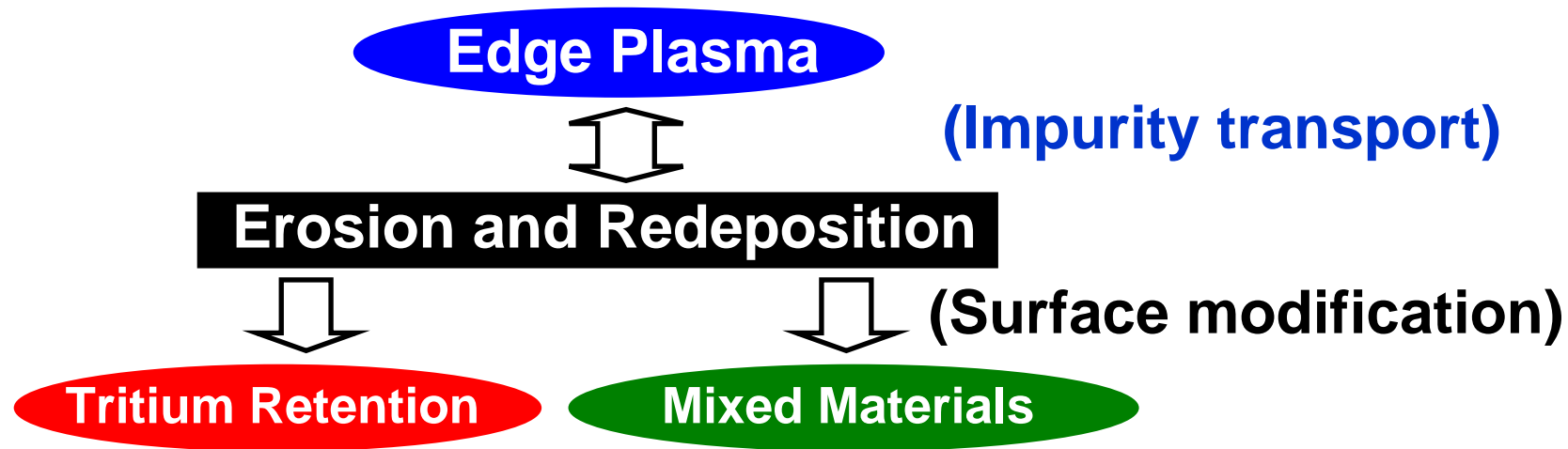
- ◎ high power deposition and erosion during edge-localized modes (ELMs) and disruption, **(wall lifetime)**
- ◎ excessive tritium inventory and control,
- ◎ the present limited understanding of mixed-materials effects, and **(wall lifetime)**
- ◎ the feasibility of using tungsten plasma-facing components.





Contents

- Present status of a dynamic Monte Carlo code, *EDDY*, which simulates materials erosion/deposition and plasma impurity transport



- Calculation results;

- (1) Dynamic erosion/deposition on tungsten due to plasmas with carbon Impurity,
- (2) Asymmetric erosion and redeposition between inner and outer divertors
- (3) Hydrocarbon redeposition in the gaps between divertor tiles and the shadowed area by the steps of neighboring tiles

- Present code development;

Molecular dynamics of low-energy particle solid interactions



Dynamic plasma surface interaction code, *EDDY*

Plasma ion irradiation on material surfaces

- (1) Simultaneous bombardment with hydrogen and impurity ions with different species and charge states ; $H^+ + Be^{q+}, C^{q+}, Fe^{q+}, Mo^{q+}, W^{q+}$, and etc.
- (2) Maxwellian velocity distribution and sheath acceleration
; $T_e = T_i$ and $V_{sh} = -(T_e/2) \ln(\pi m_e/m_i)$

Dynamic erosion and deposition processes

- (3) **Physical** sputter **erosion** and plasma carbon impurities **deposition**
- (4) **Chemical** sputter **erosion** due to hydrocarbons formation
- (5) Collisional mixing and thermal diffusion → **materials mixing**
; $10^7 \sim 10^8$ pseudo-ions for $10^{25} \sim 10^{26} \text{ m}^{-2}$
; atomic density n_{W-C} is $(n_{W-C})^{-1} = f_W(n_W)^{-1} + f_C(n_C)^{-1}$, where $f_W + f_C = 1$.
; one dimensional Fickian equation with a diffusion coefficient

Impurity transport in near-surface plasma

- (6) Multiple ionizations and dissociations of sputtered and reflected impurities, including CH_4 and higher hydrocarbons
→ **rate coefficients from Janev and Reiter**

Dynamic plasma surface interaction code, *EDDY*

- (7) Gyromotion of the ionized impurities, simultaneously receiving
 (a) collisional friction force, (b) temperature gradient thermal force,

$$F_z = m_z \frac{(v_i - v_z)}{\tau_s} + \alpha_e \frac{d(kT_e)}{ds} + \beta_i \frac{d(kT_i)}{ds}$$

- (c) crossed field diffusion, $(\Delta x, \Delta y) = \sqrt{2D_{\perp} \Delta t} \bullet (r_{Gx}, r_{Gy})$

- (d) sheath and presheath electric field,

$$\phi(z) = \phi_1 \exp\left(-\frac{z}{2\lambda_{Debye}}\right) + (\phi_0 - \phi_1) \exp\left(-\frac{z}{R_{gyro}}\right) \quad f_D = 1 - \phi(6\lambda_{Debye}) / \phi_0 \approx 0.25$$

- and (e) elastic collision with neutral hydrogen using hard sphere collisions with certain radii; virial coefficients of the Lennard-Jones potential for molecules and radii of maximum density of orbital electrons for atoms

実験室系の散乱角：

$$\theta = \arctan\left\{\frac{m \sin(\pi - 2\vartheta)}{M + m \cos(\pi - 2\vartheta)}\right\}$$

$$\vartheta = \arcsin R^{1/2}$$

M : CH_4 の質量, m : 中性H原子の質量, R : 一様乱数

衝突後と衝突前のエネルギーの比：

$$\frac{E_{after}}{E_{before}} = \frac{(M - m)^2 \cos^2 \vartheta + (M + m)^2 \sin^2 \vartheta}{(M + m)^2}$$

Local and prompt redeposition on surfaces

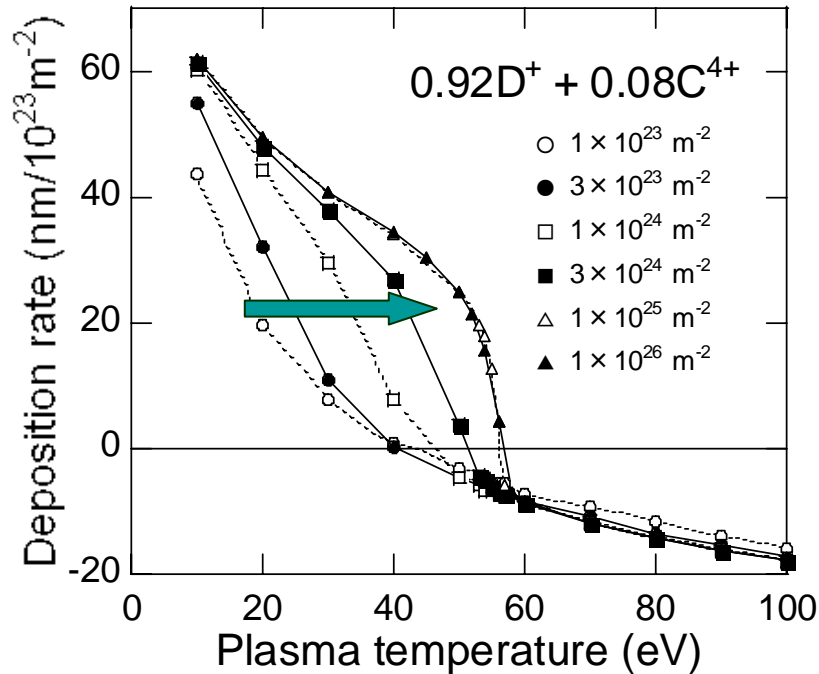
- (8) Reflection or sticking of carbon and hydrocarbons

→ **particle species- and energy-dependent coefficients from Alman and Ruzic**

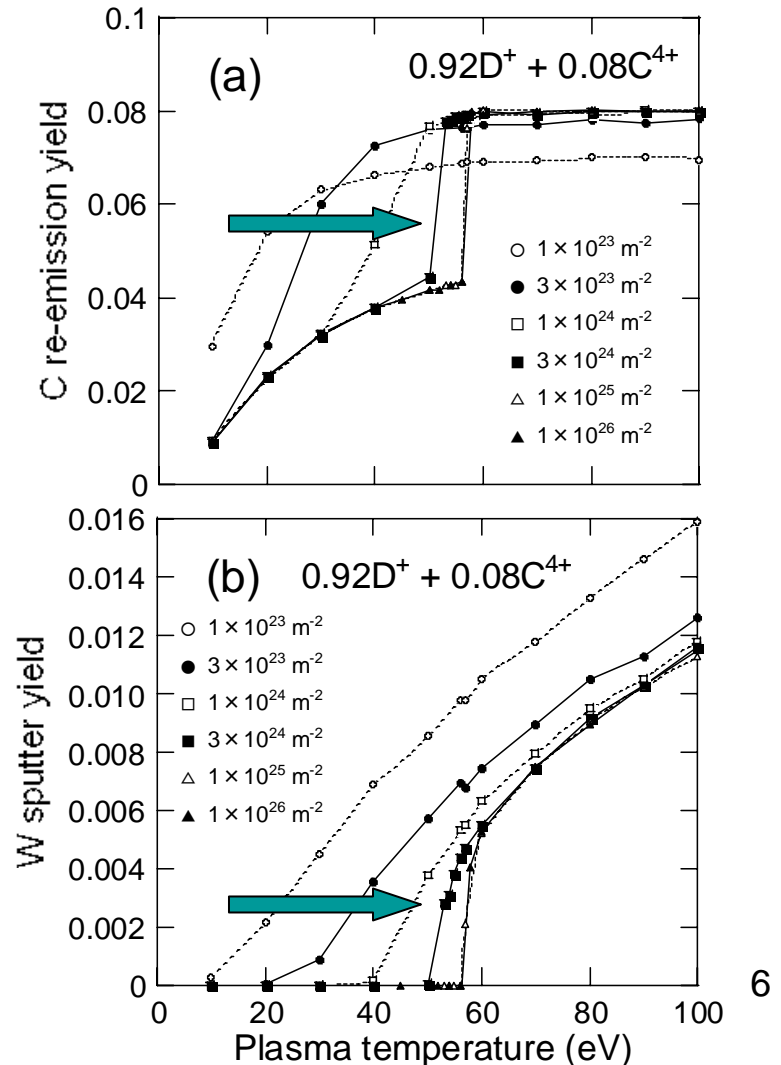
or constant sticking for each hydrocarbon.

Dynamic erosion/deposition on tungsten

Plasma temperature dependence of erosion and deposition

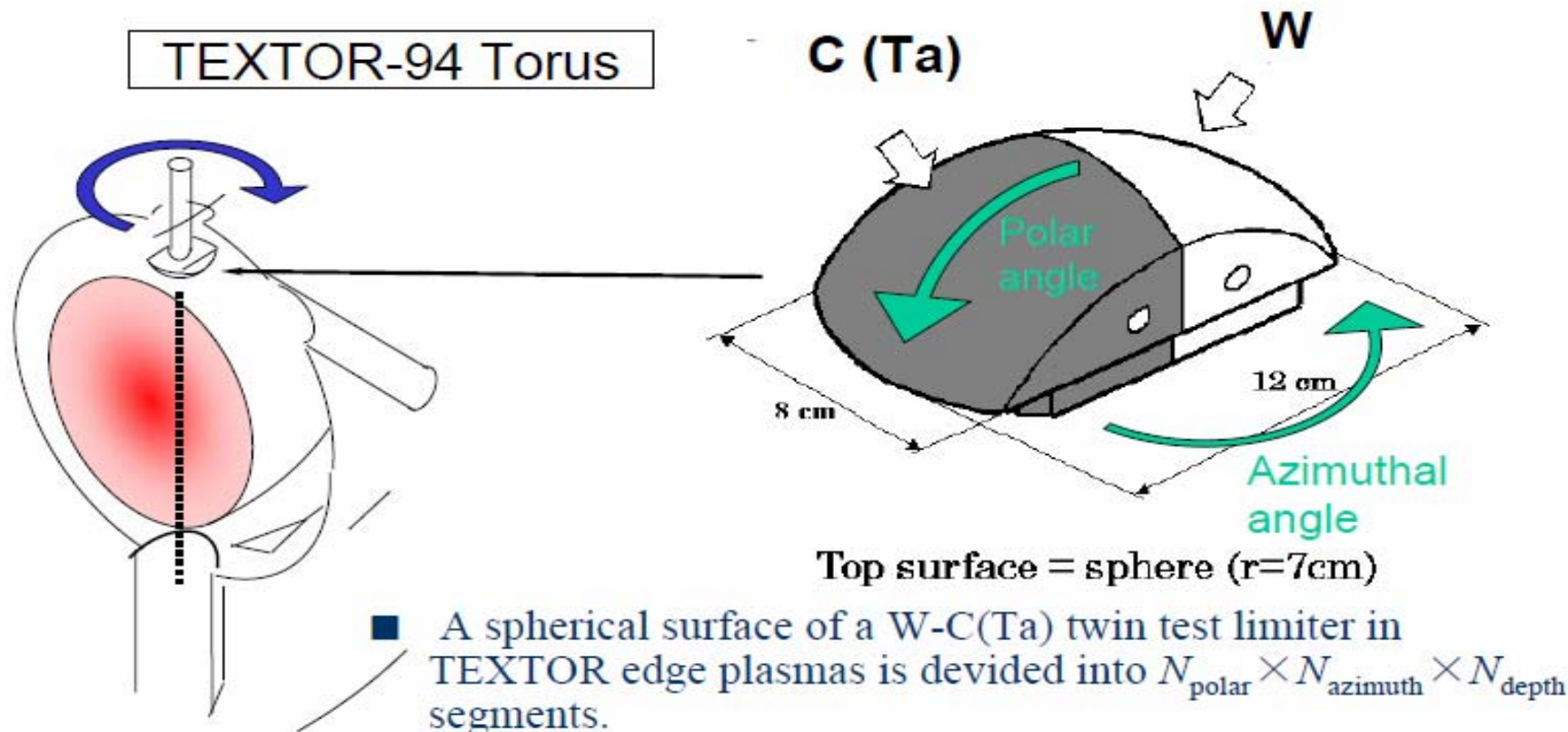


- The deposition rate changes dynamically with plasma temperature.
- Finally, a sharp transition is formed.
- The thick C layer causes the C re-emission yield to decrease at low temperature.
- Both the C and W yields approach fluence-independent values for a W-C layer.



Dynamic erosion/deposition on tungsten

■ W-C(Ta) twin test limiter experiments in TEXTOR



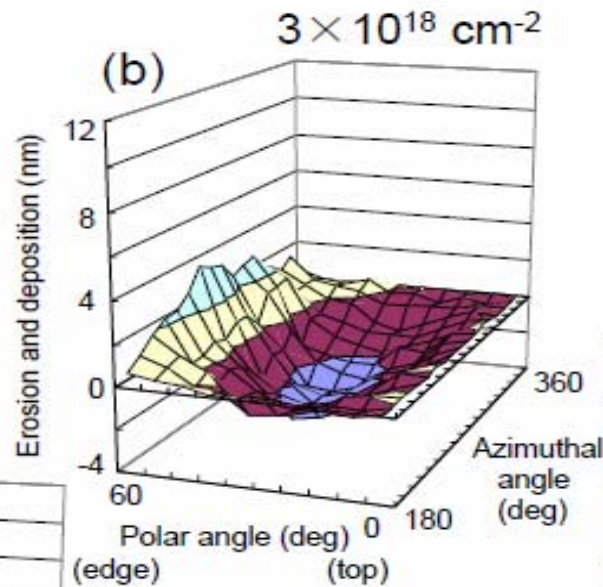
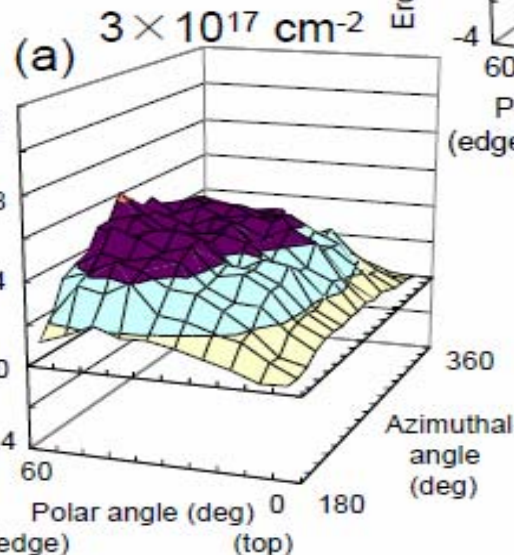
$$(N_{\text{polar}}=10, N_{\text{azimuth}}=36, N_{\text{depth}}=10)$$

- TEXTOR edge plasma (at the top of the limiter)
 - $n_e=5.2 \times 10^{12} \text{ cm}^{-3}$ ($\lambda_{ne}=3.26 \text{ cm}$); $T_e=64 \text{ eV}$ ($\lambda_{Te}=2.56 \text{ cm}$)
 - $B=2.25 \text{ T}$; $D^+ : C^{4+} = 98\% : 2\%$; $T_e=Ti$ is assumed.

Dynamic erosion/deposition on tungsten

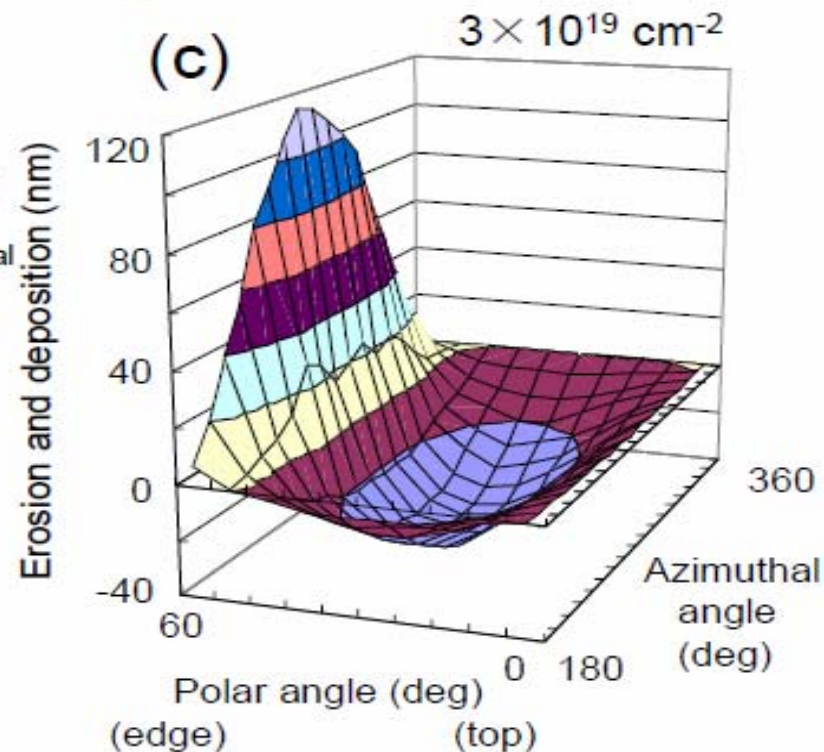
- Erosion and deposition patterns on W side of W-C twin limiter

(a) At early stage of exposure, whole W side is covered by C



(b) Both erosion and deposition zones appear on W side

(c) A sharp boundary between erosion and deposition zones is produced.



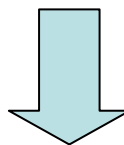
Erosion/redeposition in inner and outer divertors

- Carbon deposition profile and its hydrogen retention on plasma facing components were found to be quite dependent on the geometrical structure of the divertor, including an asymmetry between inner and outer regions.

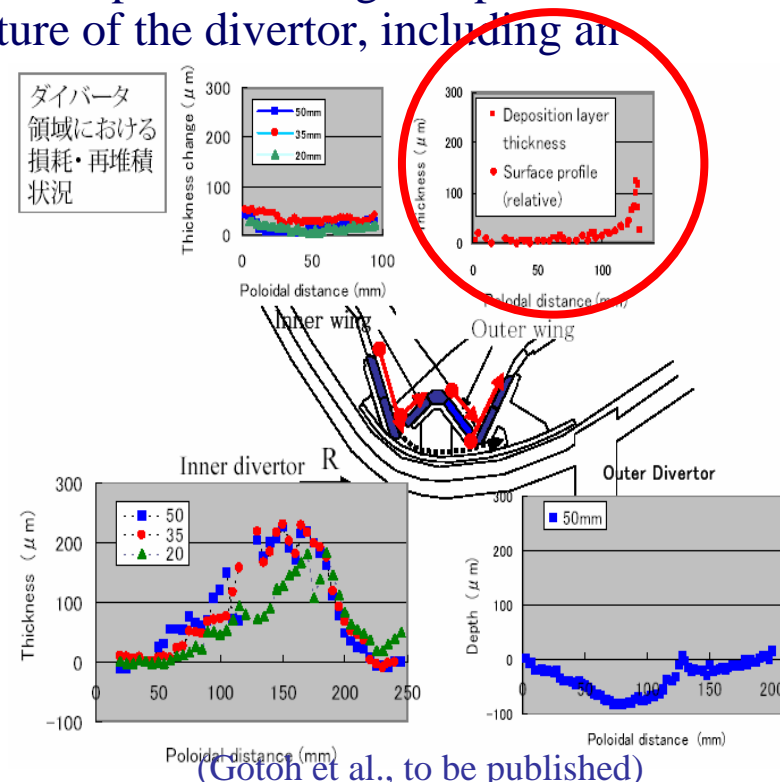
Erosion was dominant on outer divertor tiles, and deposition was dominant on inner divertor tiles.

- Such geometry effect was also observed in the outer region of W-shaped divertor in JT-60U.

Heaviest deposition on outer dome wing, which was not directly faced to plasma, was observed at the bottom edge of the wing.



- Modeling of hydrocarbon transport in the inner and outer regions of the W-shaped divertor in JT-60U is conducted in this study.

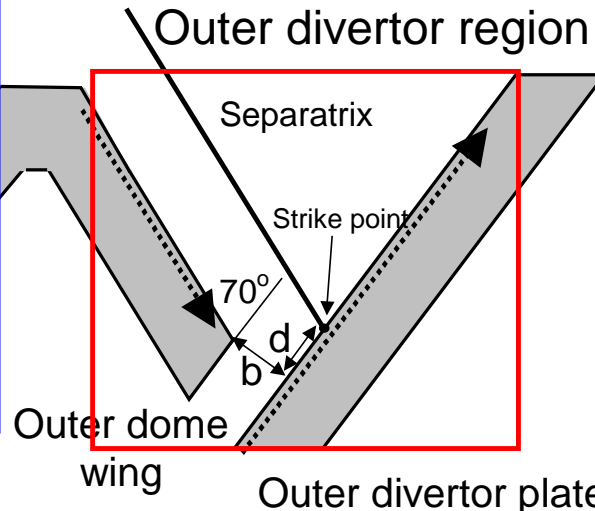
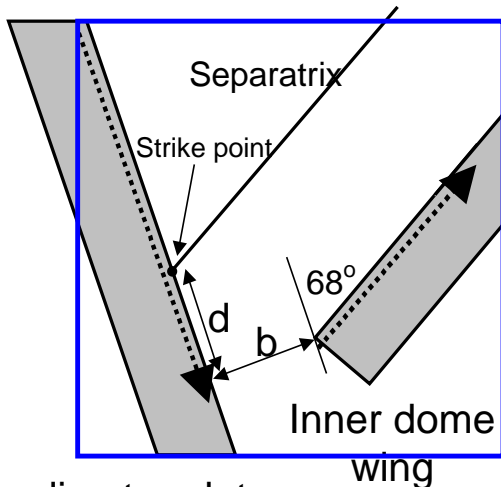


“Redeposition mechanism of carbon and hydrocarbons in the divertor”
“Origins of the in-out asymmetry in erosion and deposition patterns”

Erosion/redeposition in inner and outer divertors

Divertor model and plasma conditions

Inner divertor region



Inner divertor plate

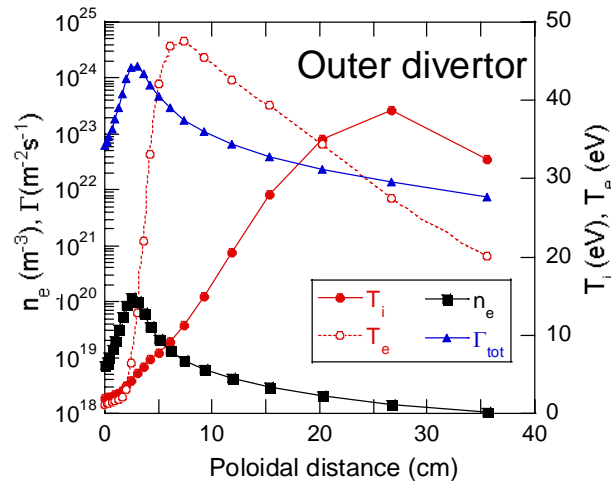
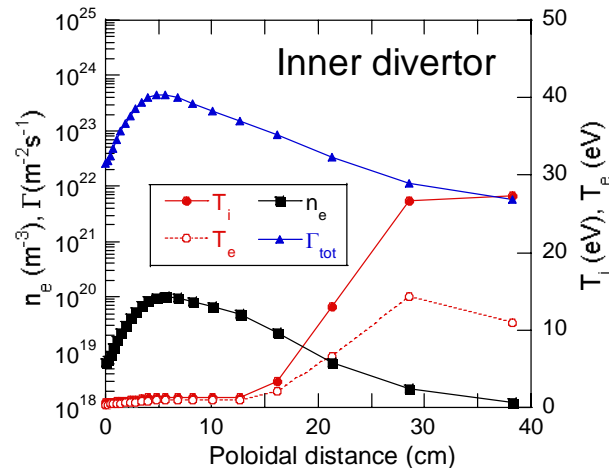
Outer divertor plate

- B_T (inner)=3 T
- B_T (outer)=2.7 T
- $\theta_{toroidal}=2^\circ$

- Plasma parameters above the divertor plates are calculated using UEDGE with a boundary condition of $n_i=10^{19} \text{ m}^{-3}$ and $P_{flow}=8\text{MW}$.

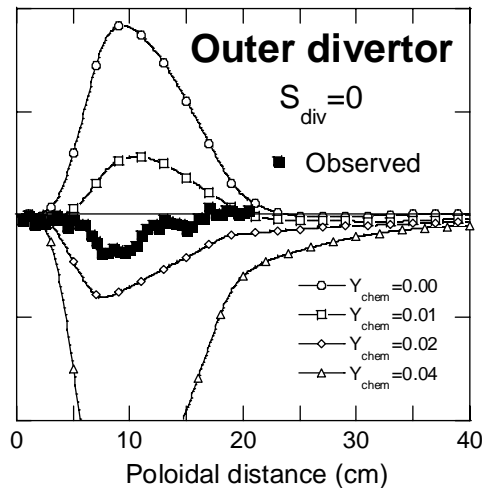
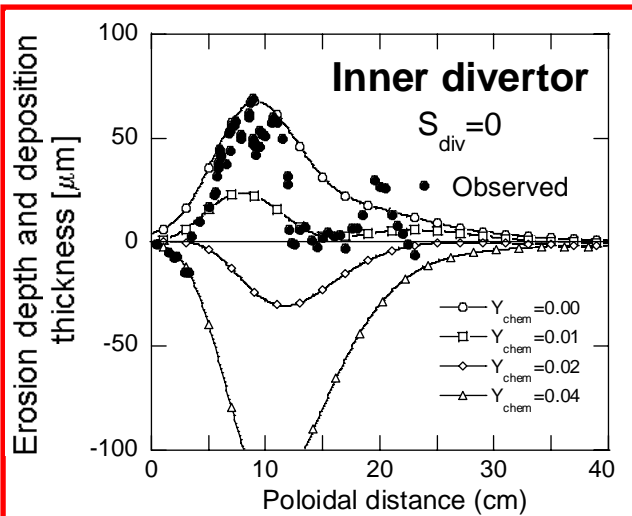
- Impurity transport from outer region to inner region is not taken into account.

- Plasma carbon concentration is higher for inner region than for outer region; at the strike point, ~2% and 0.7%, respectively.

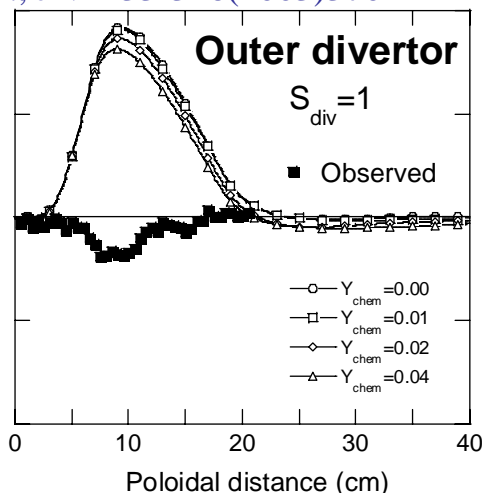
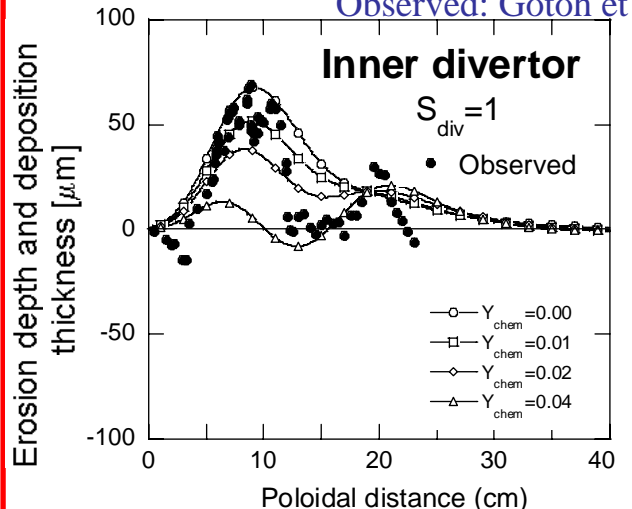


Erosion/redeposition in inner and outer divertors

Erosion and redeposition patterns on *inner* divertor plate



Observed: Gotoh et al., JNM 33-316(2003)370



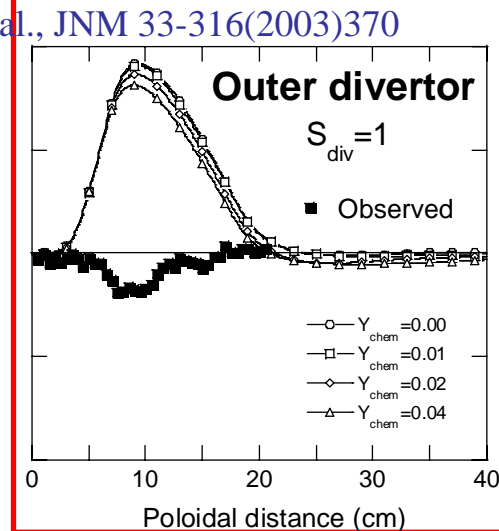
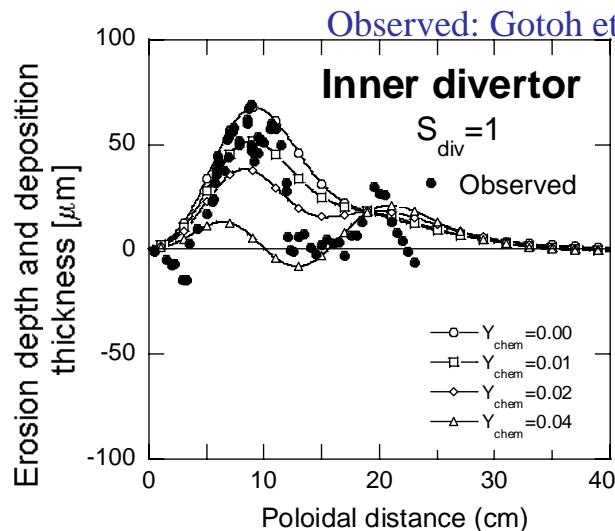
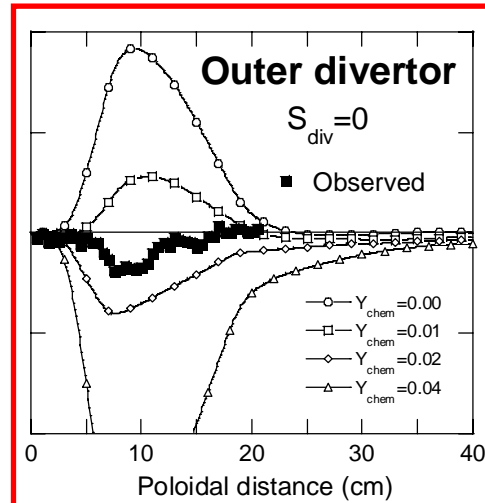
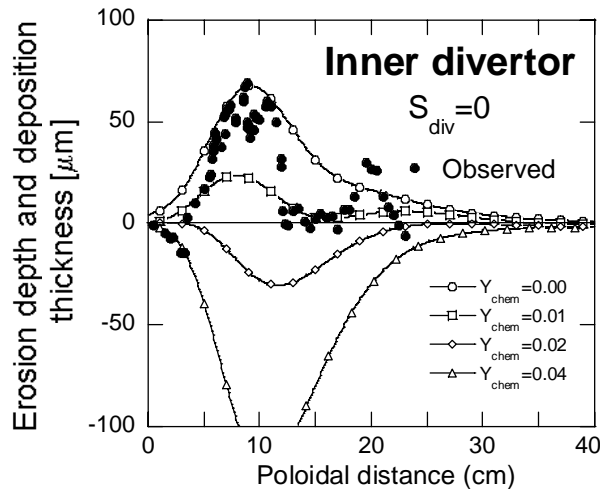
The calculated pattern with a fixed strike point was convoluted with the strike point distribution on the divertor plates in 1997~1998 experimental campaigns, although JT-60U had many kinds of discharges in the campaigns.

The pattern on the divertor plate was calculated as a function of the sticking coefficient (S_{div}) and chemical erosion yield (Y_{chem}).

The observed distribution of deposition layer thickness is explained mainly by the deposition of background plasma carbon impurities.

Erosion/redeposition in inner and outer divertors

Erosion and deposition patterns on *outer* divertor plates



Observed: Gotoh et al., JNM 33-316(2003)370

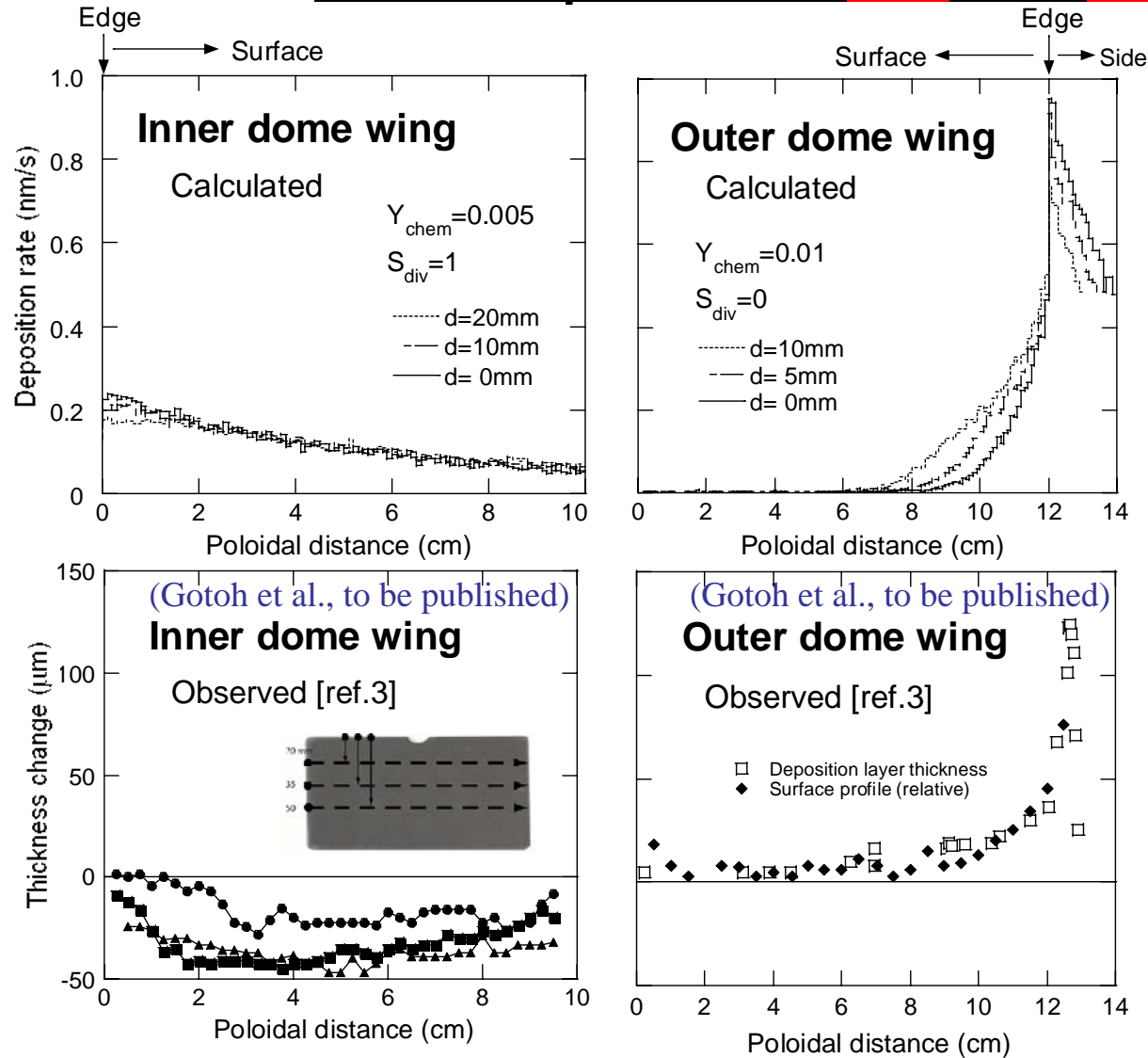
● With increasing chemical erosion yield, for zero sticking ($S_{div} = 0$), *erosion* dominates the poloidal distribution.

● For full sticking ($S_{div} = 1$), due to higher temperature of the plasma, hydrocarbons from the outer divertor plate are immediately ionized when entering into the plasma and return the surface, so that *deposition* still dominates the distribution.

Reasonable agreement of the observed erosion distribution is deduced only by the assumption of a *negligible sticking* of hydrocarbons and *erosion yield of 0.01–0.02* on the outer divertor plate.

Erosion/redeposition in inner and outer divertors

Carbon deposition on **inner** and **outer** dome wings



● Since the dome wings are not face to the plasma, *the deposition on the outer dome wing is caused by the hydrocarbons eroded at the divertor plates (?)*.

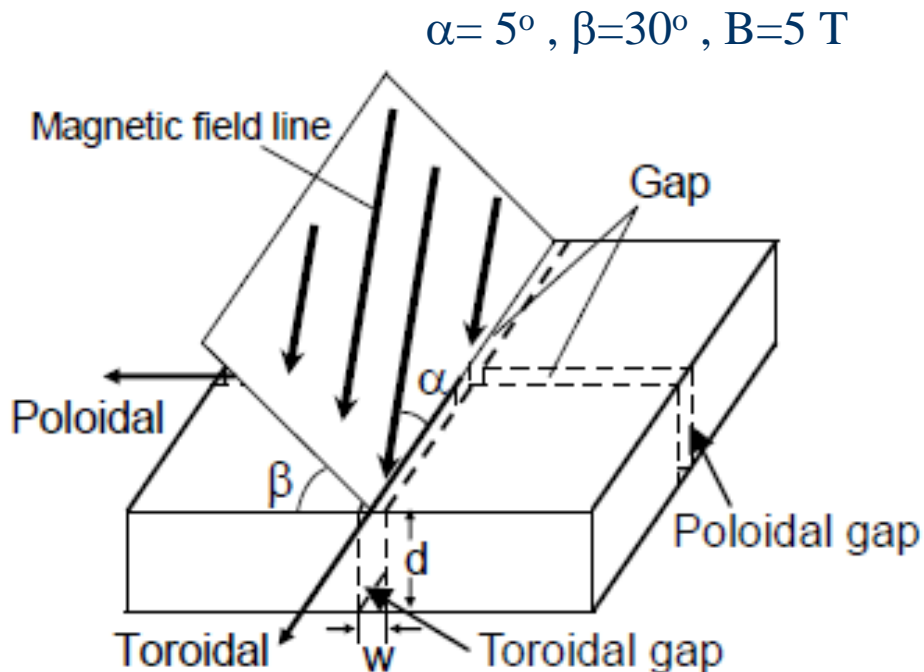
● The figures show *asymmetric poloidal deposition* of carbon/hydrocarbons between the inner and outer dome wings.

● 20 % and 10 % of hydrocarbons eroded from the divertor plates are deposited on the inner and outer dome wings, respectively.

The calculated distributions show the *local deposition at the outer wing edge and the global distribution on the whole inner wing, but an erosion on the inner wing is observed*.

Hydrocarbon redeposition in toroidal and poloidal gaps

■ Schematic view of a divertor tile geometry and surface models



(a) Toroidal and poloidal gaps between the tile ($d=20 \text{ mm}$, $w=3 \text{ mm}$)

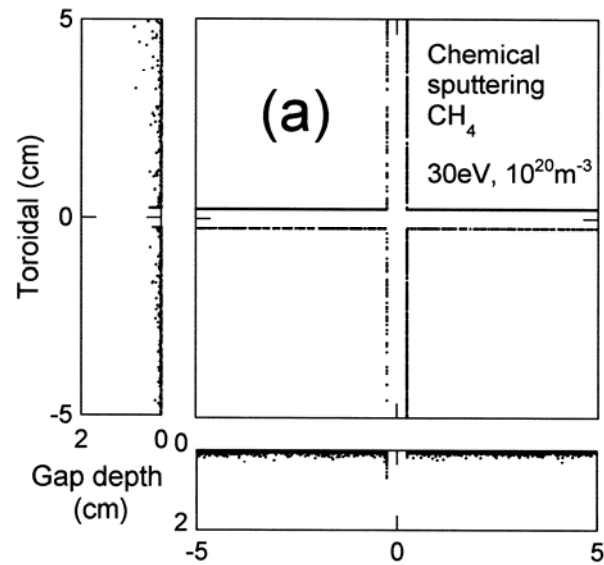
■ $10^5 \sim 10^6$ methane molecules (CH_4) are released on the top surface ($10\text{cm} \times 10\text{cm}$).

■ The transport process of hydrocarbons, including electron-impact ionization, dissociation, and dissociative recombination and charge exchange collisions, is simulated in a rectangular volume above the tile surface.

■ The energy- and species-dependent sticking coefficients (Alman and Ruzic), or constant sticking coefficients, have been used for the side surface in the gap; D.A. Alman and D.N. Ruzic: Physica Scripta T111 (2004)145.

■ No sticking of hydrocarbons on the top surface is assumed where they are released again in the form of CH_4 .

Hydrocarbon redeposition in toroidal and poloidal gaps



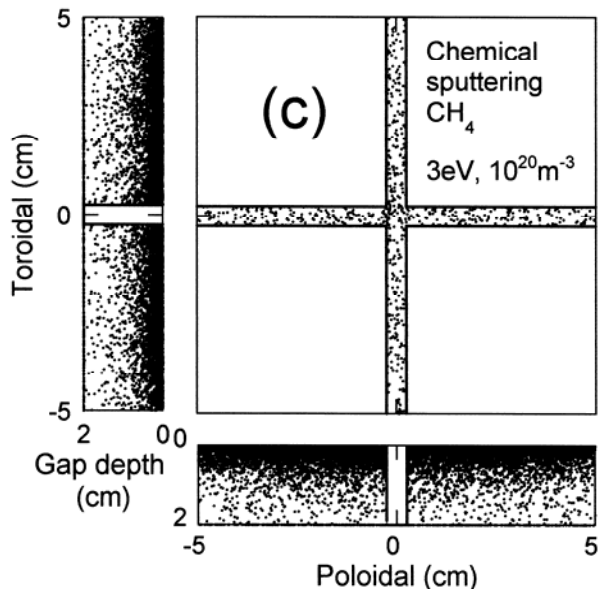
Redeposition patterns of carbon and hydrocarbon fragments in toroidal and poloidal gaps

$$\alpha = 5^\circ, \beta = 30^\circ, B = 5 \text{ T} \quad w = 5 \text{ mm}, d = 20 \text{ mm}$$

- *At high plasma temperature*, the redeposition is observed only on the shallow side in the gap and there is no redeposition on the bottom or the inner part of the gap.

- There is asymmetry in the redeposition patterns between toroidal and poloidal gaps.

- The patterns are dominated by the magnetic geometry on the tile surface.

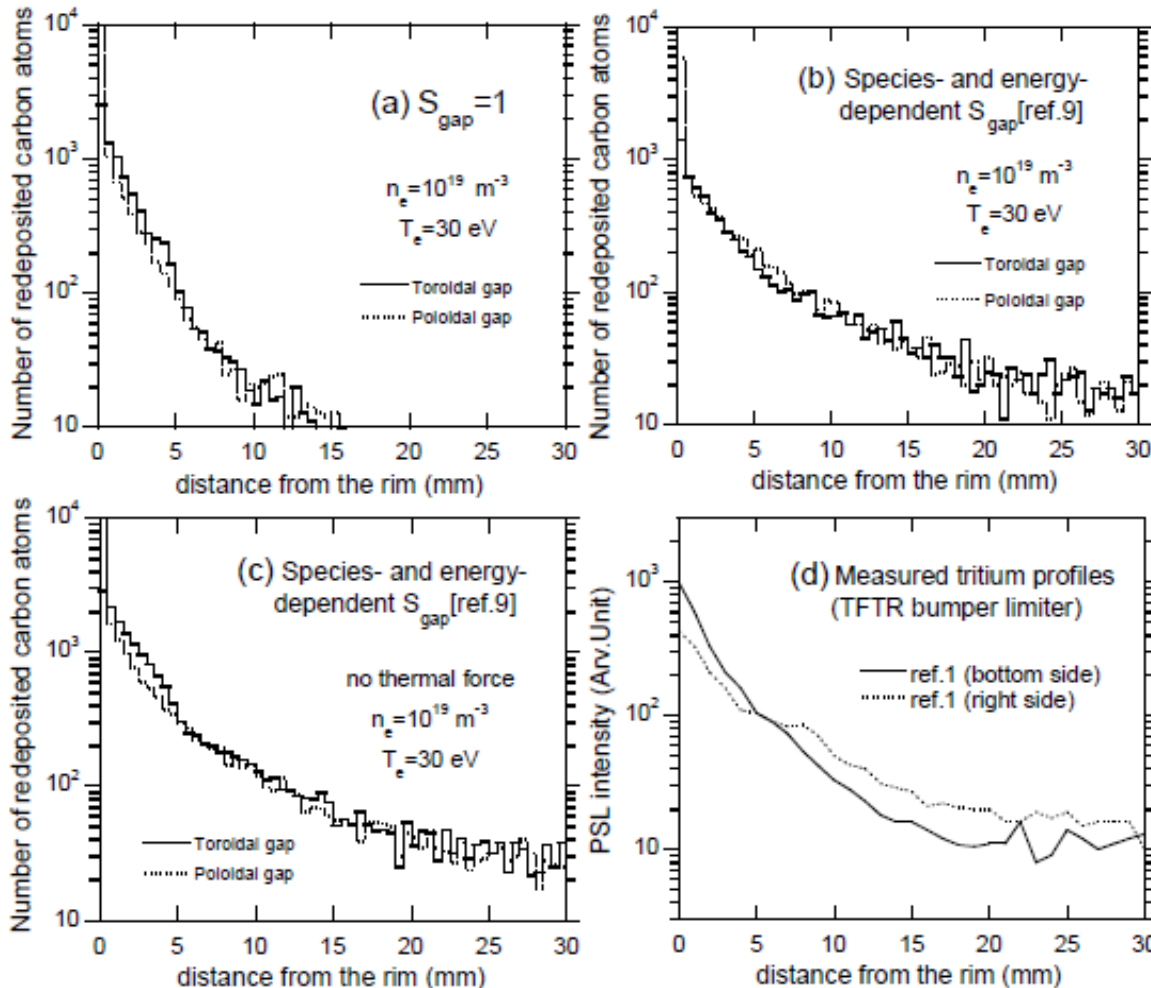


- *At low plasma temperature*, neutral species are liberated from a magnetic constrain and as a result, they randomly deposit not only on the top surface of the tiles but also in the bottom and the inner part of the gap between the tiles.

- There is no asymmetry in the redeposition patterns between the toroidal and poloidal gaps.

Hydrocarbon redeposition in toroidal and poloidal gaps

Redeposition distributions on the side surfaces of toroidal and poloidal gaps

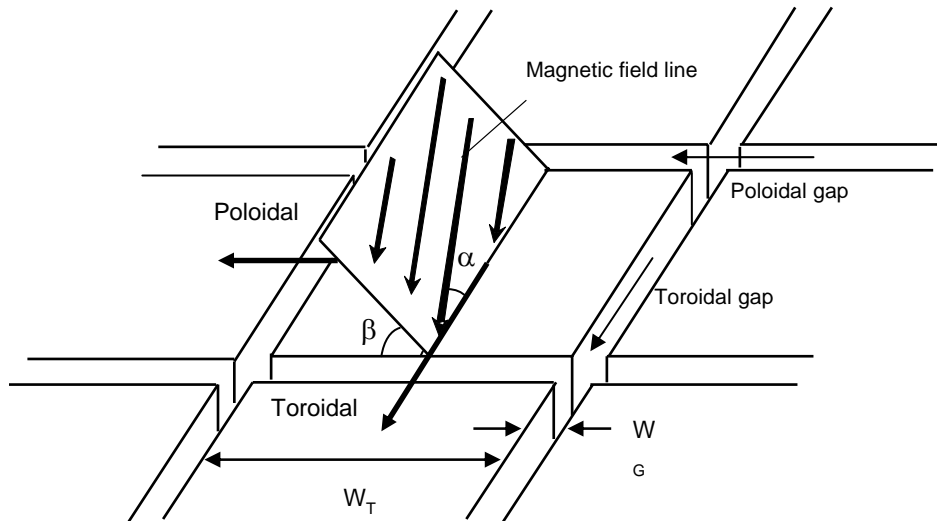


■ Using the energy dependent reflection (or sticking) coefficient of the side surface, low-energy hydrocarbons subsequently reflected at the side surface redeposit deeply in the gap.

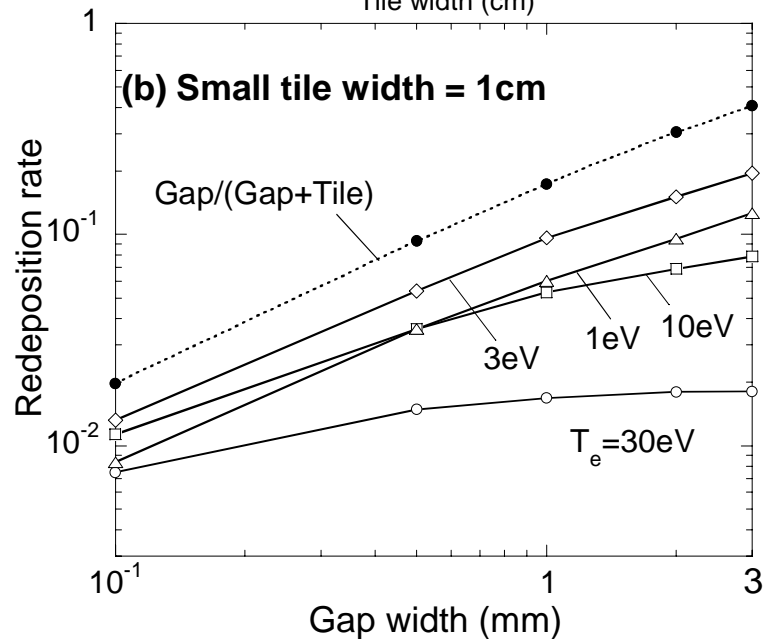
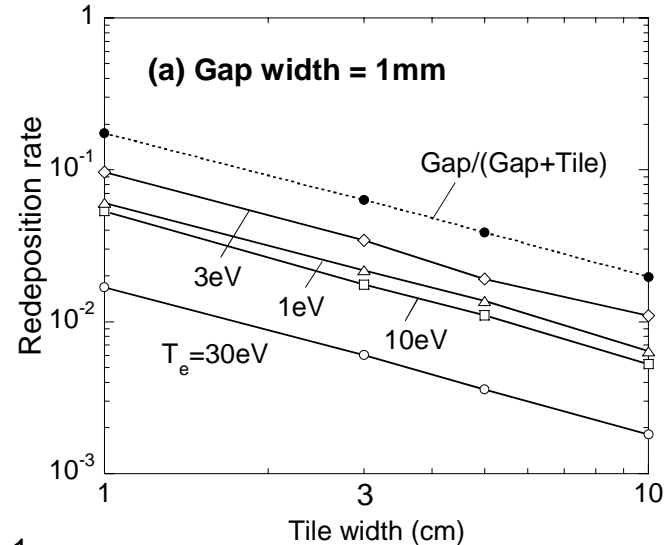
■ The calculated results show similar distribution of the observed short and long decay lengths of the bumper limiter tile used in TFTR [8].

[8] T. Tanabe et al., Fusion Sci. Technol. 48 (2005) 577.

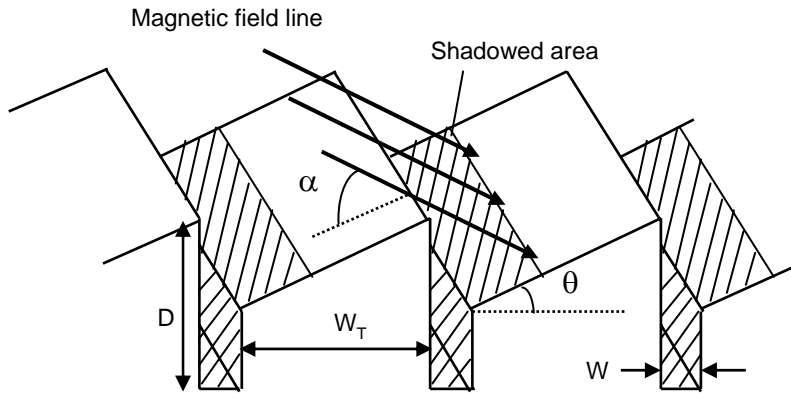
Hydrocarbon redeposition in castellated surfaces



- *Periodic boundary conditions* are introduced to the single gap model.
- At temperatures of the order of eV, the deposition rate increases with increasing gap width.
- At higher temperatures, due to dominant *prompt redeposition*, it tends to be independent of the gap width.

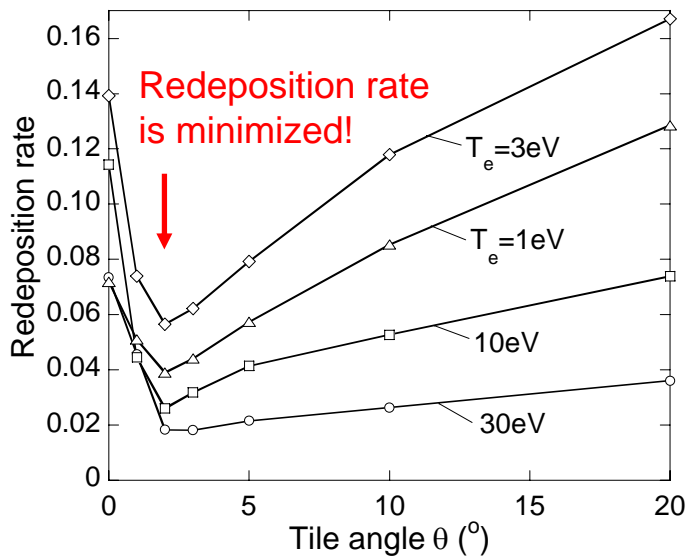


Hydrocarbon redeposition at plasma shadowed area



$D=15\text{mm}$
 $W_T=10\text{mm}$
 $W_G=1\text{mm}$
 $\alpha=20\text{deg.}$
 $B=5\text{T}$

Whole region (gap+shadowed) hidden from direct access

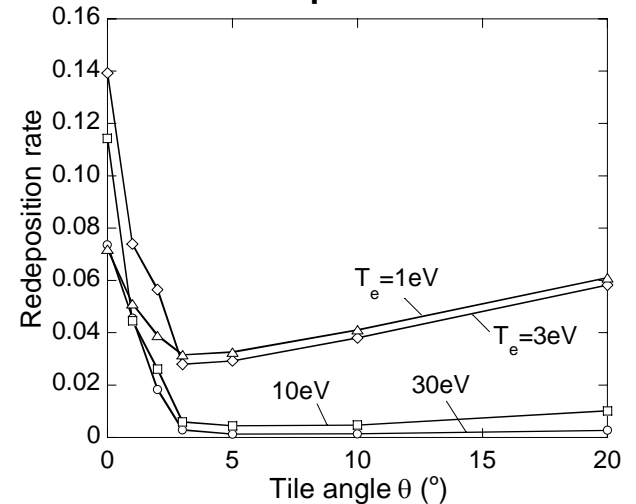


■ With increasing angle, the deposition in the gap is strongly suppressed

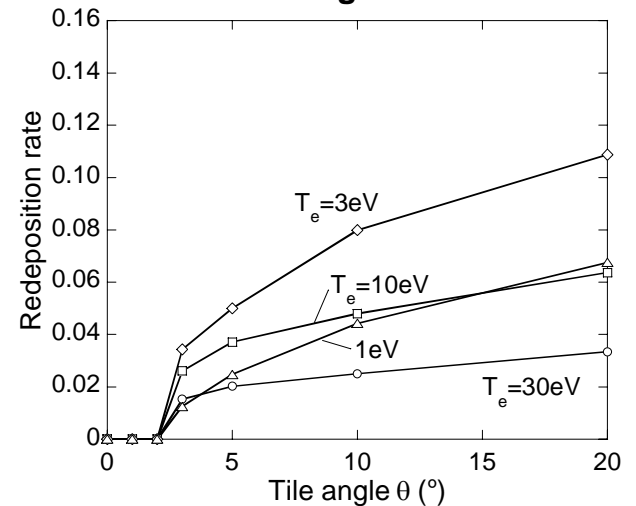
■ most of hydrocarbons are deposited on the shadowed area, which gradually increase.

■ Therefore, there is an angle that the deposition is minimized.

Gap sides



Shadowed region on the tile



* More detailed discussion including redeposition distributions and species will be presented at the PET-11 conference (P2-21)

Molecular dynamics simulation of ion-solid interactions

- Modified Brenner potential functions are used for W-C-H system;

$$V = \sum_{\alpha\beta} \left(A \exp(-\lambda_A r^{\alpha\beta}) - \underbrace{\bar{b}}_{\text{bond-order}}^{\alpha\beta} B \exp(-\lambda_B r^{\alpha\beta}) \right)$$

N. Juslin P. Erhart, P. Traskelin, J. Nord, K. O. E. Henriksson, E. Salone, K. Nordlund, and K. Albe, J. Appl. Phys. 98, 123520 (2005)

- Kinetic equations are solved using the Leap-Frog method modified the Verlet algorithm.

- Velocity scaling method for temperature control.

H.J.C. Berendsen, J.P.M. Postma, E.F. van Gunsteren, A. DiNola, and J.R. Haak; J. Chem. Phys., 1984. **81** 3684.

- Multi Time step; $\Delta t = 1/100 \times$ (Flight time for Lattice constant)

- 2D periodic boundary conditions

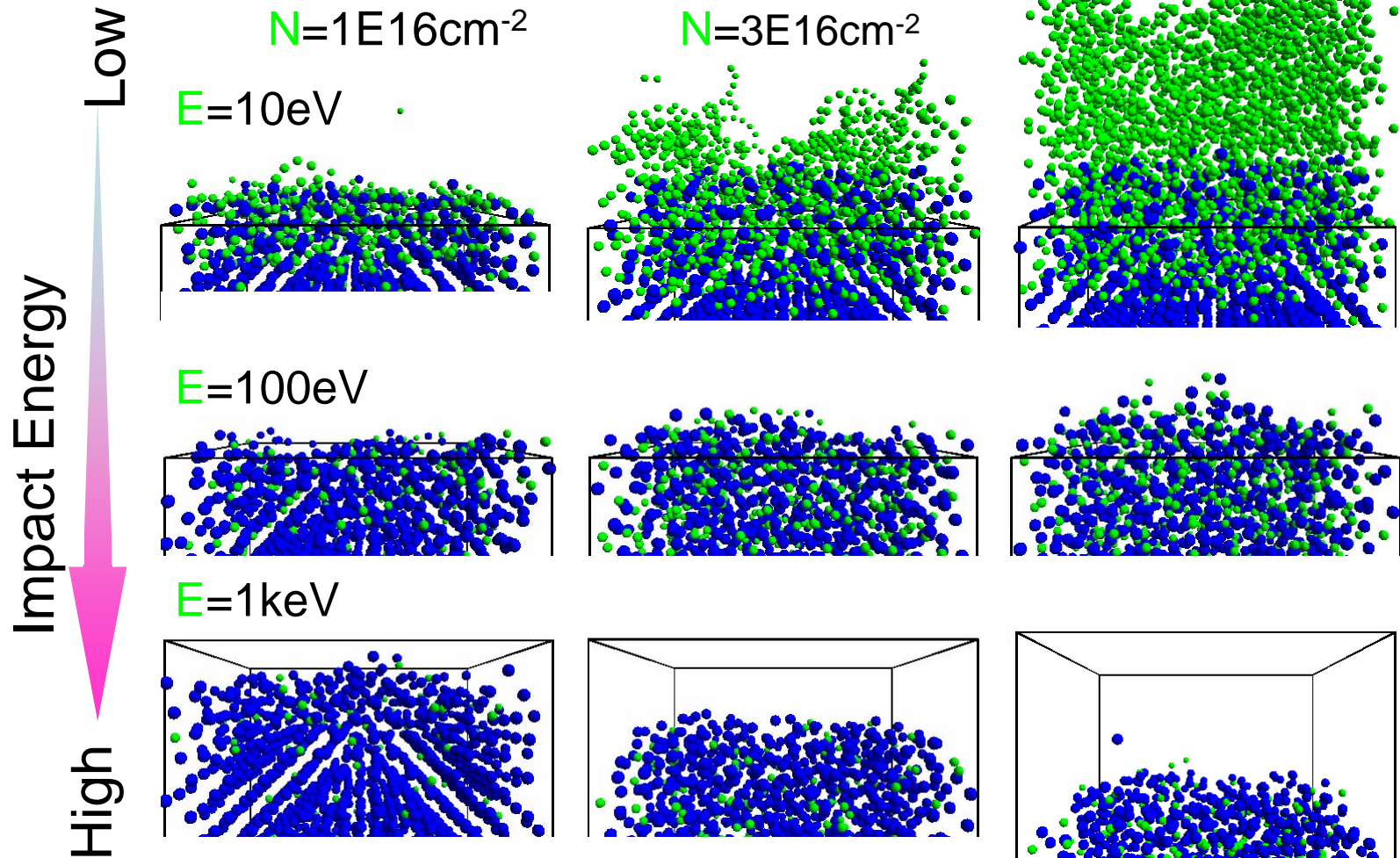
Molecular dynamics simulation of ion-solid interactions

C → W

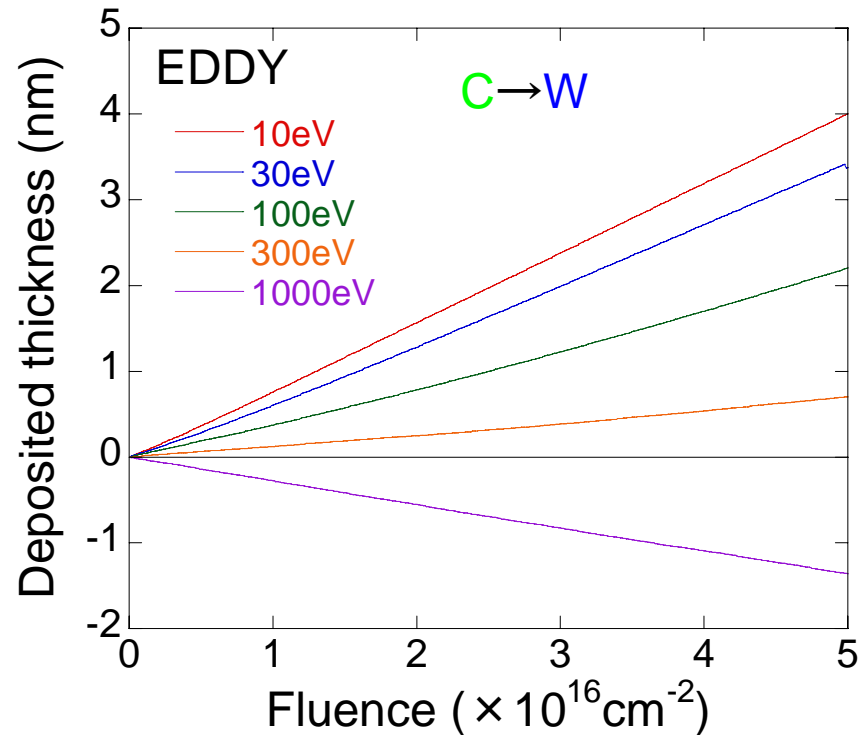
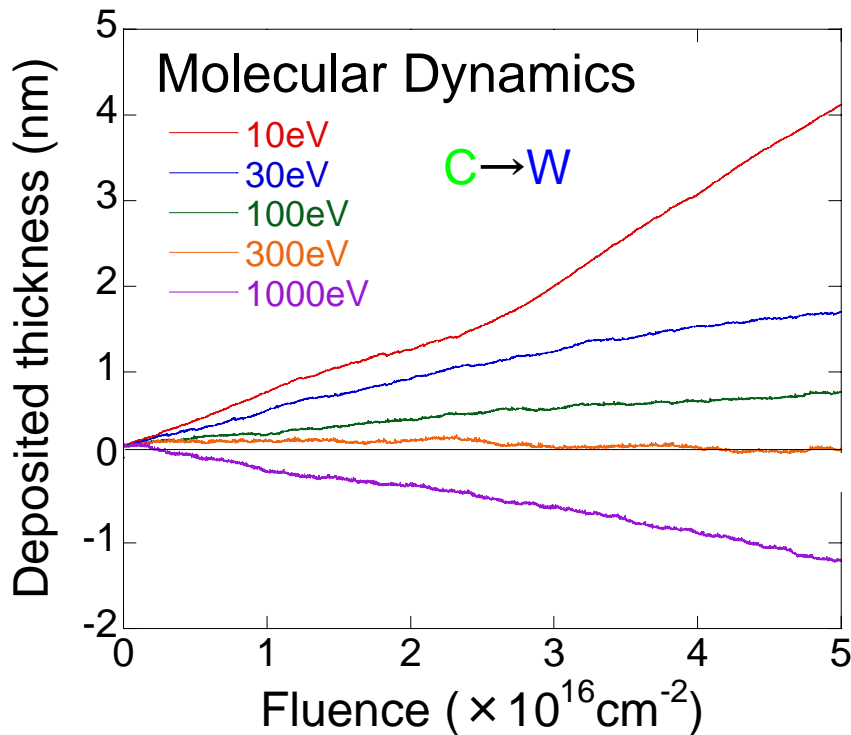
Ion fluence

Low

High
 $N=5E16cm^{-2}$

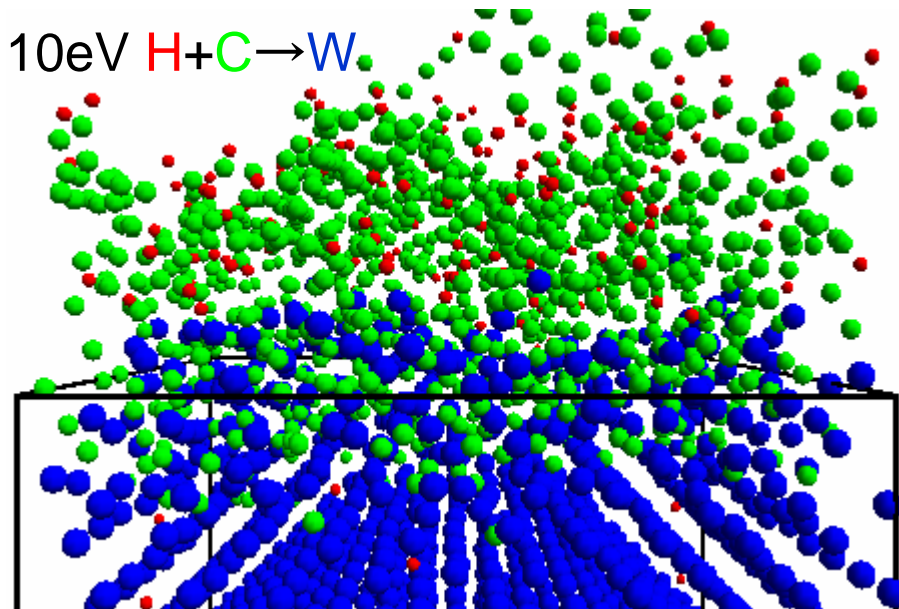


Fluence and energy dependence of erosion and deposition on W



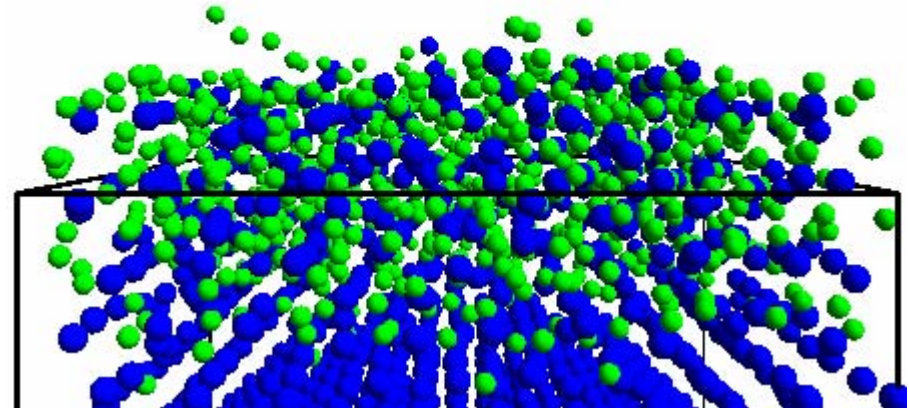
■ Calculated erosion and carbon depositions linearly depend on the fluence, which is in agreement with the EDDY calculations.

Simultaneous bombardment of W with H and C ions



H: $2E16cm^{-2}$, C: $2E16cm^{-2}$

10eV $C \rightarrow W$

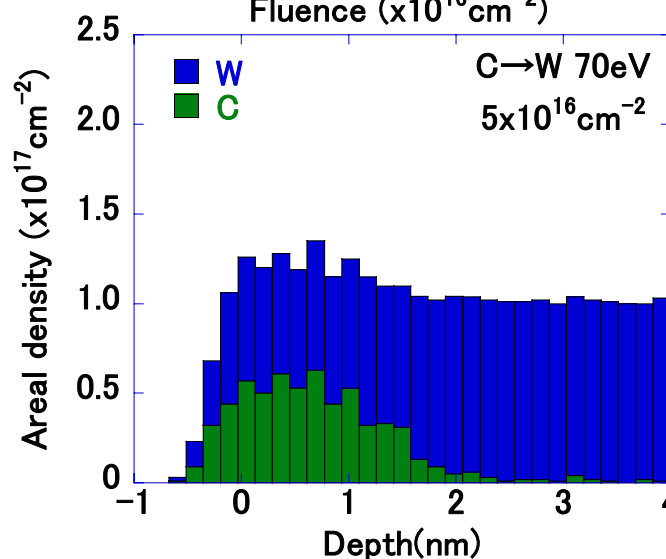
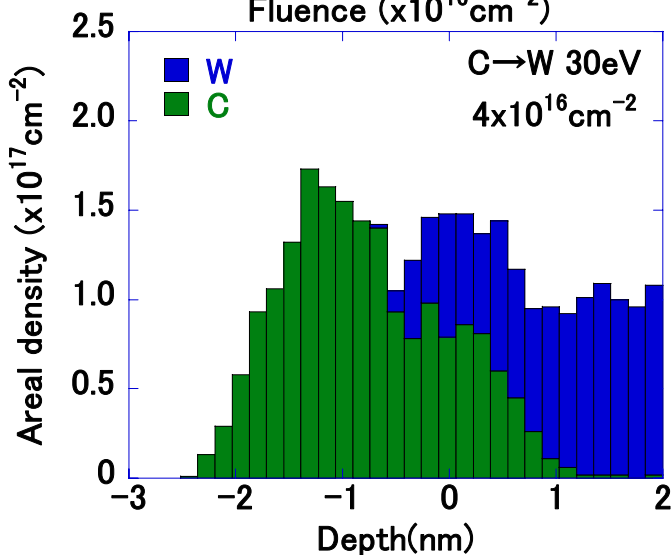
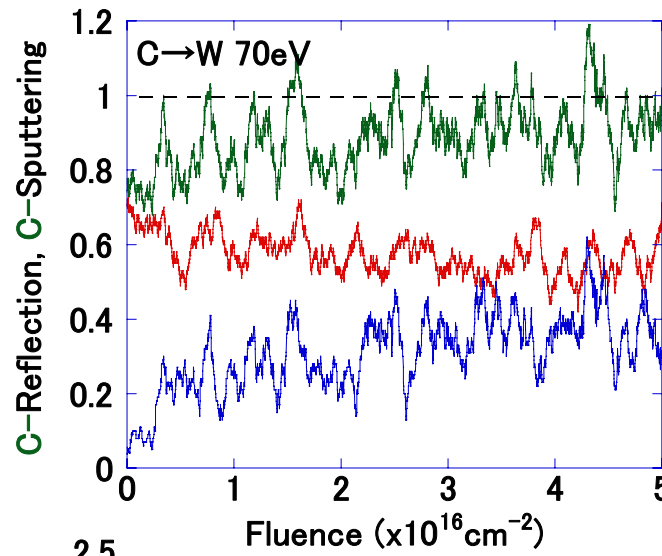
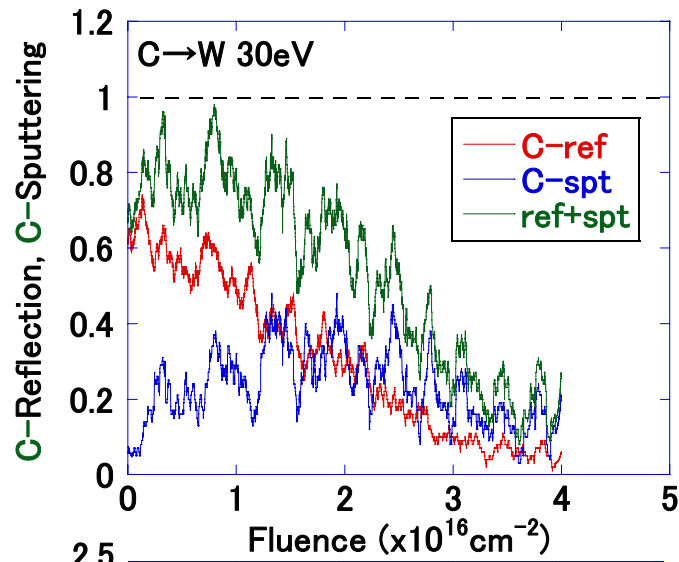


H: 0, C: $2E16cm^{-2}$

■ For simulation of plasma ion bombardment, we use Maxwellian distributed ions with different temperatures.

■ Simultaneous bombardment with hydrogen and C ions changes the C deposition thickness on W

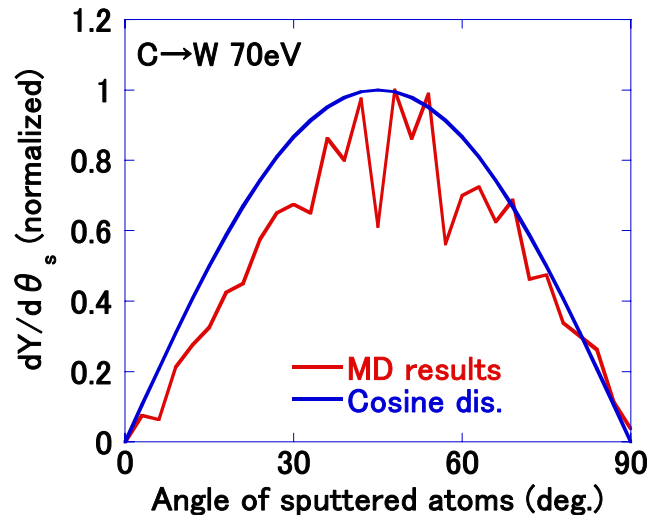
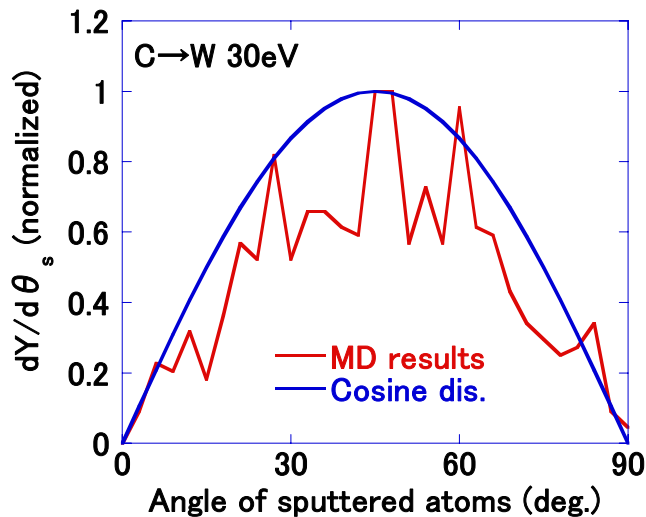
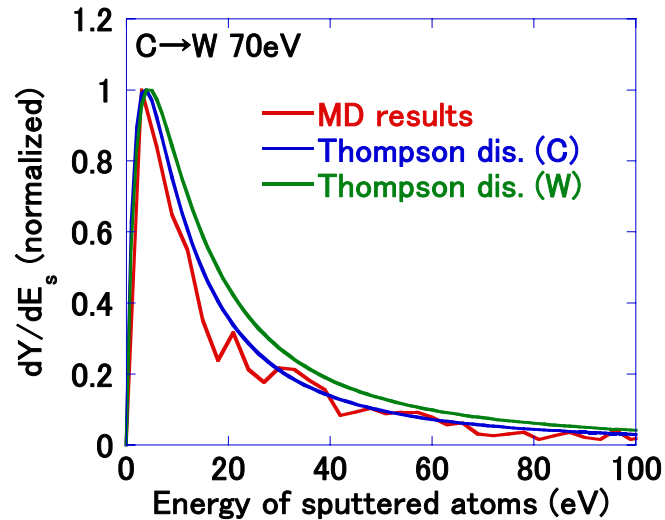
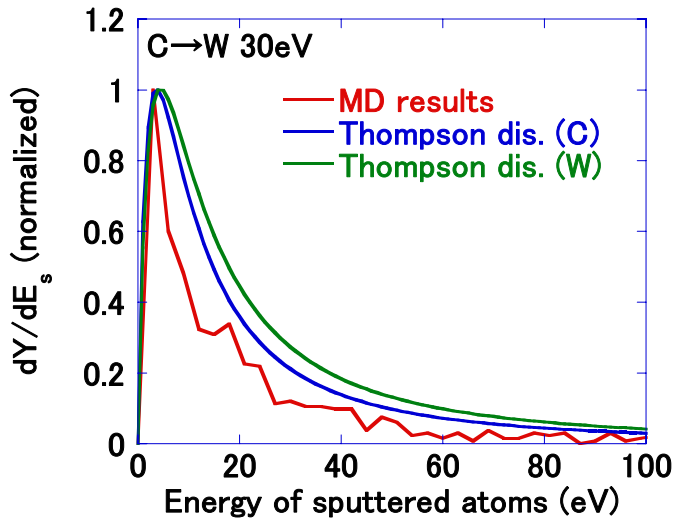
Fluence dependence on C-reflection and C-sputtering from W



At low plasma temperature, the reflection of C ions decrease due to C deposition on W. **A thick C-rich layer is produced.**

At high temperatures, a **W-C mixed layer is produced on the surface**, where a steady-state condition is reached. The C emission yield approaches one.

Energy and angular distributions of sputtered C atoms



■ With increasing plasma temperature, the energy distribution becomes the *Thompson distribution*.

■ The angular distribution approaches the *cosine distribution*.



Thank you very much
for your attention